Thermoelectric properties of a double quantum dot out of equilibrium in Kondo and intermediate valence regimes

D. Perez Daroca,[1,2] P. Roura-Bas,[3,2] and A. A. Aligia[4]
[1]*Gerencia de Investigación y Aplicaciones, GAIDI, CNEA, 1650 San Martín, Buenos Aires, Argentina*
[2]*Consejo Nacional de Investigaciones Científicas y Técnicas, 1025 CABA, Argentina*
[3]*Centro Atómico Bariloche, GAIDI, 8400 Bariloche, Argentina*
[4]*Instituto de Nanociencia y Nanotecnología CNEA-CONICET, GAIDI, Centro Atómico Bariloche and Instituto Balseiro, 8400 Bariloche, Argentina*

(Received 15 June 2023; revised 3 September 2023; accepted 29 September 2023; published 10 October 2023)

We study a system composed of two quantum dots connected in series between two leads at different temperatures, in the limit of large intratomic repulsion. Using the noncrossing approximation, we calculate the spectral densities at both dots $\rho_i(\omega)$, the thermal and thermoelectric responses, thermopower, and figure of merit in different regimes. The interatomic repulsion leads to finite heat transport even if the hopping between the dots $t = 0$. The thermopower can be very large compared to single-dot systems in several regimes. The changes in sign of the thermoelectric current can be understood from the position and magnitude of the Kondo and charge-transfer peaks in $\rho_i(\omega)$. The figure of merit can reach values near 0.7. The violation of the Wiedemann-Franz law is much more significant than in previously studied nanoscopic systems. An analysis of the widths of $\rho_i(\omega)$ indicates that the dots are at effective temperatures T_i intermediate between those of the two leads, which tend to be the same for large t.

DOI: 10.1103/PhysRevB.108.155117

I. INTRODUCTION

During the last two decades, the study of nanodevices that convert heat into work has received great attention due to possible applications [1]. In particular, thermoelectric properties in transport through single molecules [2–7] and quantum dots [8–11] has been experimentally studied. Usually, these systems can be modeled by the single impurity Anderson model, or its generalizations to multilevel systems, and the thermal properties of these models, in and out of equilibrium, have been addressed by several calculations [5,8,12–33]. Particularly in recent years, these studies have been extended to systems of two quantum dots or molecules [30,34–44].

For linear response (in the limit of vanishing voltage and thermal gradient) the numerical renormalization group (NRG) has been used to calculate the relevant quantities, like the electrical and thermal conductances or the thermopower (Seebeck coefficient S) [17,31,32,34,37,44–46]. The NRG is a robust numerical technique. However, out of equilibrium, for a finite bias voltage or difference of temperature between the conducting leads, NRG is very difficult to apply (although some developments using the scattering states NRG approach look promising [45,46]) and different approximations have been used to capture the essential physics of the Kondo effect [47], which is always present in nanostructures for large on-site repulsion U and degenerate configurations of the localized electrons (like odd numbers of electrons in one quantum dot). In its simplest and more usual realization, the Kondo effect can be described as the screening of a localized spin by the surrounding free conduction electrons forming a many-body singlet.

Among the different approximations widely used to treat Kondo systems out of equilibrium, one can mention equations of motion (EOM) for the Keldysh-Green functions [16,26,48–51], renormalized perturbation theory (RPT) in U or similar Fermi-liquid approaches [21,28,29,39,52–60], slave bosons in the mean-field approximation (SBMFA) [24,36,61–65], noncrossing approximation (NCA) [41,66–75], auxiliary master equation approach [76,77], or other renormalization procedures [78–80]. Recently, a method that combines NRG with time-dependent density matrix renormalization has been used [81]. All traditional methods have limitations. The EOM does not reproduce correctly the functional dependence of the energy scale T_K on the on-site energy E_d [49,50]. RPT is valid for small energies and it is not easy to apply to more complex systems. The SBMFA with increasing temperature [47] or magnetic field [82] has an abrupt artificial transition to a phase in which the impurity decouples from the conduction band. The NCA does not satisfy Fermi-liquid relations at zero temperature, and when the ground-state configuration of the isolated impurity (or system disconnected to the conducting leads) is nondegenerate (like for positive E_d for one impurity or nonzero magnetic field), the impurity self- energy has an unphysical positive imaginary part at low temperatures and as a consequence the spectral density presents a spurious peak at the Fermi energy [66]. For finite U the NCA ceases to reproduce correctly the dependence of T_K with parameters and vertex corrections should be included [83–85].

Using the SBMFA, Sierra *et al.* studied a system of two Kondo impurities (modeling two quantum dots in a serial arrangement) under a thermal bias [36]. They find some unusual results, like negative differential thermal conductance and sign reversal of the thermoelectric current for certain

parameters. Taking into account the limitations mentioned above for the SBMFA at finite temperature, it is convenient to check these results with an independent technique. We study the same system (including also interdot Coulomb repulsion) using the NCA. In spite of the shortcomings mentioned above, the NCA is known to reproduce correctly the relevant energy scale T_K and its dependence on the different parameters. It has proved to be a very valuable tool for calculating the differential electrical conductance through different systems [67] such as two-level quantum dots and C_{60} molecules displaying a quantum phase transition [68–70], a nanoscale Si transistor [71], or vibrating molecules [72,73], among others [41,74]. It also reproduces correctly the scaling of the conductance for small bias voltage V and temperature T [75].

Regarding the accuracy of the NCA within the linear response regime, we note that a comparative study of the numerical renormalization group and NCA results for the spectral functions has been done [86]. In particular, they have shown (Fig. 7 of Ref. [86]) that the NCA spectral functions at temperatures $T \geqslant 0.1T_K$ are reliable enough to compute transport properties. As for the nonequilibrium results at equal chemical potentials, the same is true if the temperature of the cold lead is kept at a similar condition, that is $T_R \geqslant 0.1T_K$.

Our paper is a comprehensive study of different regimes of the double quantum dot (DQD) system, although restricted to the situation with inversion symmetry for simplicity. Among our most peculiar results, we find unusually large and small Lorenz numbers compared to those found usually in metals, semimetals, alloys, degenerate semiconductors [87], and other nanoscopic systems [15,27]. Also in some cases large figure of merits ZT are obtained and in other cases, large thermopower. Analyzing the width of the spectral densities of both dots, we show that they can be interpreted as each dot is at an intermediate temperature between that of the left and the right leads. For interdot hopping $t \to 0$ each dot is at equilibrium with the corresponding lead, while at large t they are at nearly the same intermediate temperature.

The paper is organized as follows. In Sec. II, the model, the methods and the expressions for the electrical and heat current are presented. The results for the occupancy of the DQD fluctuating between 0 and 1 particles and between 1 and 2 particles are showed in Secs. III A and III B, respectively. Section IV is devoted to the summary and discussion. The NCA treatment of fluctuations between 1 and 2 particles in the DQD is discussed in Appendix A. Finally, in Appendix B, an alternative expression for the calculation of the charge current is described in detail.

II. MODEL AND METHODS

A scheme of the system out of equilibrium is shown in Fig. 1. It is composed by a DQD where each dot is tunnel-coupled to a metallic reservoir. The Hamiltonian describing the system is the following:

$$H = H_{DQD} + H_c + H_V. \tag{1}$$

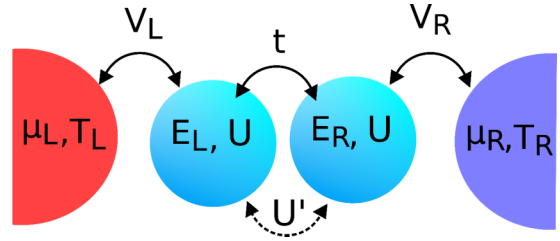

FIG. 1. Scheme of the system.

The first term describes the DQD,

$$H_{DQD} = \sum_{\nu\sigma} E_\nu d^\dagger_{\nu\sigma} d_{\nu\sigma} + \sum_\nu U n_{\nu\uparrow} n_{\nu\downarrow} + U' \sum_{\sigma\sigma'} n_{L\sigma} n_{R\sigma'} - t \sum_\sigma (d^\dagger_{L\sigma} d_{R\sigma} + \text{H.c.}), \tag{2}$$

where E_ν and U (U') are the energy levels and the intra-(inter-) dot Coulomb repulsion respectively, $\nu = \{L, R\}$ labels the left and right dot (and leads) and $\sigma = \uparrow, \downarrow$ stands for the spin projection. The hopping energy between dots is represented by t.

The second term describes the conducting leads

$$H_c = \sum_\nu H_\nu = \sum_{k\nu\sigma} \varepsilon_{\nu k\sigma}\, c^\dagger_{\nu k\sigma} c_{\nu k\sigma}, \tag{3}$$

and the last one, describes the hybridization between each dot and its respective lead

$$H_V = \sum_{k\nu\sigma} (V_{k\nu}\, d^\dagger_{\nu\sigma} c_{\nu k\sigma} + \text{H.c.}). \tag{4}$$

In order to treat the system within the NCA and avoid the need to consider vertex corrections, we diagonalize H_{DQD} and retain only two neighboring configurations, which correspond to the limit $U \to +\infty$. In this way, the problem is mapped into a multilevel system connected to two conducting leads. With some adequate change of phases, the model is electron-hole symmetric. Therefore there are two independent cases to be considered: fluctuations between 0 and 1 particles in the DQD and fluctuations between 1 and 2 particles. Thus, It suffices to retain the eigenstates and energies of H_{DQD} for 1 and 2 particles.

We assume for simplicity that the DQD has inversion symmetry. Therefore, $E_L = E_R \equiv E_d$. The eigenstates for 1 particle are the even and odd linear combinations

$$d^\dagger_{e\sigma} = \frac{1}{\sqrt{2}}(d^\dagger_{L\sigma} + d^\dagger_{R\sigma}), \quad E_e = E_d - t,$$
$$d^\dagger_{o\sigma} = \frac{1}{\sqrt{2}}(d^\dagger_{L\sigma} - d^\dagger_{R\sigma}), \quad E_o = E_d + t. \tag{5}$$

It is easy to see that in the new basis, the problem of fluctuations between 0 and 1 particles has the same form as the interference one studied before with level splitting $\delta = 2t$ [73,88,89].

Regarding the two-particle sector, the four relevant eigenstates for $U - U' \to +\infty$ correspond to an even singlet and an odd triplet. In the notation $|Sm\rangle$ of the total spin and its

projection, they are

$$\begin{aligned}|00\rangle &= \frac{u}{\sqrt{2}}(d^\dagger_{L\uparrow}d^\dagger_{R\downarrow} - d^\dagger_{L\downarrow}d^\dagger_{R\uparrow})|0\rangle \\ &\quad + \frac{v}{\sqrt{2}}(d^\dagger_{L\uparrow}d^\dagger_{L\downarrow} + d^\dagger_{R\uparrow}d^\dagger_{R\downarrow})|0\rangle, \\ |11\rangle &= d^\dagger_{L\uparrow}d^\dagger_{R\uparrow}|0\rangle, \\ |10\rangle &= \frac{1}{\sqrt{2}}(d^\dagger_{L\uparrow}d^\dagger_{R\downarrow} + d^\dagger_{L\downarrow}d^\dagger_{R\uparrow})|0\rangle, \\ |1-1\rangle &= d^\dagger_{L\downarrow}d^\dagger_{R\downarrow}|0\rangle,\end{aligned} \tag{6}$$

where to linear order in t, $u = 1$, and $v = 2\chi$ with $\chi = t/(U - U')$. The energy of the degenerate triplet is $E_1 = 2E_d + U'$ and the corresponding one for the singlet is $E_0 = E_1 - J$ with $J = 4t^2/(U - U')$.

In the new basis, the problem for fluctuations between 1 and 2 particles takes the form

$$H_{1-2} = \sum_{\xi\sigma} E_\xi |\xi\sigma\rangle\langle\xi\sigma| + \sum_{Sm_S} E_S |S,m\rangle\langle S,m| + H_c + H_V, \tag{7}$$

where $\xi = \{e, o\}$ and $S = 0, 1$ and $-S \leqslant m \leqslant S$. In this representation, the hybridization term of Eq. (4) takes the form

$$H_V = \sum_{k\nu\sigma}\sum_{\xi\sigma'}\sum_{Sm} V_{k\nu}\, D^{Sm,\xi\sigma'}_{\nu\sigma}|S,m\rangle\langle\xi\sigma'|c_{\nu k\sigma} + \text{H.c.}, \tag{8}$$

where the matrix elements $D^{Sm,\xi\sigma'}_{\nu\sigma} = \langle S,m|d^\dagger_{\nu\sigma}|\xi\sigma'\rangle$, are given in Appendix A together with a brief explanation of the NCA treatment.

In what follows, we summarize the conventions and expressions of the charge and heat currents used in this work. Treating the system of Fig. 1 as an interacting region coupled to conducting leads, the charge and energy currents are given by $J^\nu_C = -e\langle\dot{N}_\nu\rangle$, $J^\nu_E = -\langle\dot{H}_\nu\rangle$ and $J^\nu_Q = J^\nu_E - \mu_\nu J^\nu_C$, with e the absolute value of the electronic charge and $N_\nu = \sum_{k\sigma} c^\dagger_{\nu k\sigma}c_{\nu k\sigma}$. Current conservation implies $J^L_{C,E} = -J^R_{C,E}$ and if $\mu_R = \mu_L$, $J^L_Q = -J^R_Q$. In this paper we assume $\mu_R = \mu_L = 0$. Therefore, the term proportional to μ_ν vanishes and we have $J^\nu_Q = J^\nu_E$. Furthermore, after a sign associated to each flow is chosen, the index ν can be dropped from the definition of the currents. We take as positive the currents that flow from the left to the right lead. Following a procedure similar to that described in the Appendix of Ref. [89] the charge and heat currents are given by the following expressions in terms of the physical Keldysh-Green functions obtained from the NCA approximation

$$\begin{aligned}J_C = \frac{ie}{h}\int d\omega\, \text{Tr}[&(\mathbf{\Gamma^L} f_L(\omega) - \mathbf{\Gamma^R} f_R(\omega))\mathbf{G}^>_{\mathbf{d}}(\omega) \\ &+ (\mathbf{\Gamma^L} f_L(-\omega) - \mathbf{\Gamma^R} f_R(-\omega))\mathbf{G}^<_{\mathbf{d}}(\omega)],\end{aligned} \tag{9}$$

$$\begin{aligned}J_Q = \frac{ie}{h}\int d\omega\, \omega\text{Tr}[&(\mathbf{\Gamma^L} f_L(\omega) - \mathbf{\Gamma^R} f_R(\omega))\mathbf{G}^>_{\mathbf{d}}(\omega) \\ &+ (\mathbf{\Gamma^L} f_L(-\omega) - \mathbf{\Gamma^R} f_R(-\omega))\mathbf{G}^<_{\mathbf{d}}(\omega)],\end{aligned} \tag{10}$$

where

$$\mathbf{\Gamma^L} = \Gamma_L\begin{pmatrix}1 & 1\\ 1 & 1\end{pmatrix}, \quad \mathbf{\Gamma^R} = \Gamma_R\begin{pmatrix}1 & -1\\ -1 & 1\end{pmatrix} \tag{11}$$

are the matrices that couple the even and odd levels to the left and right reservoirs. Furthermore $\Gamma_\nu = \pi V^2_\nu/D$ where $2D$ represents the conduction band width and $f_\nu(\omega) = [1 + \exp[(\omega - \mu_\nu)]/k_BT_\nu]^{-1}$ is the Fermi function. We note that since $\mathbf{\Gamma^L}$ and $\mathbf{\Gamma^R}$ are not proportional, it is not possible to eliminate the nonequilibrium Green functions in the expressions of the current, and even in the linear response regime, we have to use the full nonequilibrium formalism and obtain electric and thermal conductances deriving numerically the corresponding currents. In addition, NRG approaches in the linear response regime, in which the conductances are related to the spectral density and its derivative [17], are not applicable in this case.

In Ref. [89] it was proved that the NCA is a charge current conserving approximation for a two level Anderson model. Here we have verified that the same is true for the energy (and heat in the present case) current.

For $t = 0$, the system is disconnected and it is not possible to transfer particles between both dots. Therefore, the electric current vanishes (but not necessarily the heat current as it is shown in Fig. 17). The use of the above expression for the electric current becomes numerically inaccurate for small t, because it requires the cancellation of large positive and negative terms. This fact has been also found in the interference problem [73,88]. To avoid this problem, we have derived an alternative expression for the charge current which is explicitly proportional to t and therefore, is more accurate for small t. The derivation is included in Appendix B. The result is

$$\begin{aligned}J_C &= \frac{2\pi et}{h}\sum_\sigma\int d\omega\, \text{Re}(G^<_{eo,\sigma}(\omega)) \\ &= \frac{2\pi et}{h}\sum_\sigma\int d\omega\, \text{Re}(G^<_{LR,\sigma}(\omega)).\end{aligned} \tag{12}$$

III. RESULTS

A. Fluctuations between 0 and 1 particles in the system

Here we assume that not only U is very large but also U' is sufficiently large to avoid occupancy of more than one particle in the double-dot system. The case in which the total number of particles in the system fluctuates between 3 and 4 particles can be mapped to the specific case treated in this section by an electron-hole transformation and change of sign of all the operators at the left or right part of the system.

We take the Fermi energy $\epsilon_F = 0$ as the origin of one-particle energies and assume $E_d < 0$. The problem becomes equivalent to that of transport through one dot or a molecule with two levels which interfere destructively in the transport [73,88,89]. Several mappings were discussed in Ref. [73]. In the limit $t \to 0$ the spectral density for each dot tends to that of the SU(4) Anderson model (with spin and "orbital" degeneracy), with a narrow peak of half width $\sim T_K^{\text{SU(4)}}$ at energy also $\sim T_K^{\text{SU(4)}}$ above the Fermi level and a broad charge transfer peak centered at E_d and width [90] 4Δ, where $T_K^{\text{SU(4)}}$ is the Kondo temperature of the SU(4) Anderson model, and Δ is the resonant level width. The spectral density of the SU(4) Anderson model showing both peaks is represented for example in Fig. 1 of Ref. [91]. As t increases, the even and odd one-particle states split being the former the one of

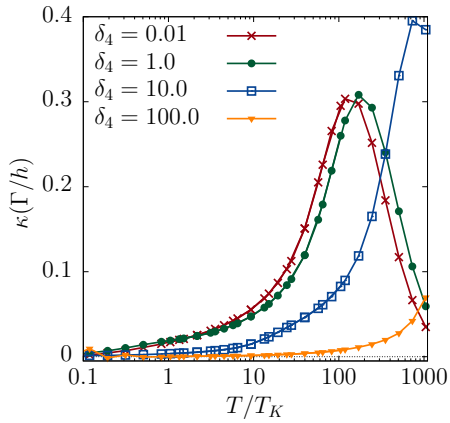

FIG. 2. Thermal conductance as a function of temperature for several values of δ_4.

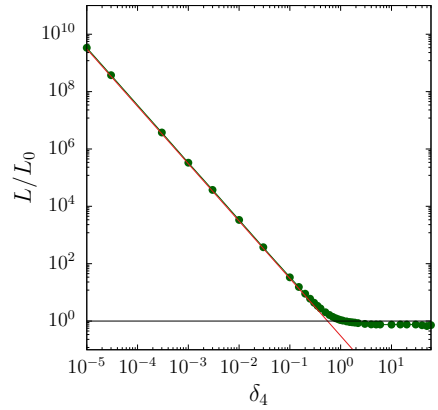

FIG. 3. Lorentz number as a function of δ_4, at $T = 0.8T_K$.

lowest energy (see Sec. II). For splitting $\delta > T_K^{\mathrm{SU}(4)}$ the density of states of the even state tends to the corresponding one of the SU(2) model with a charge transfer peak of width 2Δ [90] and a Kondo peak slightly above $\epsilon_F = 0$ of half-width $T_K^{\mathrm{SU}(2)} \ll T_K^{\mathrm{SU}(4)}$ [91,92]. The spectral density of the odd state displays a peak at energy $2t$ instead of the Kondo peak [92].

The electrical conductance $G = dI/dV$ of the model has been studied before [73,88]. It vanishes (as expected) for $t = 0$ and for large t and zero temperature, it tends to the value $G_0 = 2e^2/h$ characteristic of the SU(2) Kondo model, with a crossover when $\delta \sim T_K^{\mathrm{SU}(4)}$. The decay of G with increasing temperature resembles that expected for an SU(4) or an SU(2) model depending on the ratio $\delta_4 = \delta/T_K^{\mathrm{SU}(4)}$ [92]. Near the crossover also the occupancies of the even and odd combinations change from being nearly equal (slightly below 1/2 adding both spins) in the SU(4) regime, to be dominated by the even one in the SU(2) regime [88].

To study thermoelectric effects, we take $\Gamma = \Gamma_L + \Gamma_R = 1$ as the unit of energy, $E_e = E_d = -4$ and $E_o = E_e + \delta$, where $\delta = 2t$. We also choose the half-band width $D = 10$. For these parameters, from the equation $G(T_K)/G(0) = 1/2$, for $\delta \to 0$, we estimate $T_K^{\mathrm{SU}(4)} = 0.011$, using the variational equation [88,92]

$$T_K = \{(D+\delta)D\exp[\pi E_d/(2\Delta)] + \delta^2/4\}^{1/2} - \delta/2, \quad (13)$$

with $\delta = 0$ and this value is used in the definition of $\delta_4 = \delta/T_K^{\mathrm{SU}(4)}$ below. The Kondo temperature that enters in Figs. 2 to 7 is given by Eq. (13).

In Fig. 2 we show the thermal conductance κ in the linear response regime as a function of temperature for several splittings. In contrast to the electrical conductance, the thermal conductance increases strongly with increasing temperature for temperatures of the order of $T_K^{\mathrm{SU}(4)}$ in particular for small δ_4 (in the SU(4) regime, where the Kondo peak is clearly above the Fermi energy). As δ_4 increases beyond 1, the system enters the SU(2) regime, where the spectral density near the Fermi energy is more electron-hole symmetric, and κ is markedly reduced.

For temperatures above the charge-transfer gap $|E_d|$, the thermal conductance is expected to decrease. This seems to happen at energies below $|E_d| \sim 364T_K^{\mathrm{SU}(4)}$ for small δ_4 (for which $T_K \sim T_K^{\mathrm{SU}(4)}$). This is probably an effect of destructive interference.

A remarkable result is that while the Lorenz number $L = \kappa/(TG)$ tends approximately to the free electron value $L_0 = \pi^2/3(k_b/e)^2$, in the SU(2) regime, it diverges as δ_4^{-2} as $\delta_4 \to 0$. This fact is illustrated in Fig. 3. We are not aware of other systems with a similar property. This is a peculiar violation of the Wiedemann-Franz law. Previous violations obtained by calculations in nanoscopic systems were by factors below 5 [15,27].

For small δ this result can be understood as follows. At $T = V = 0$, the conductance G_0 is given in terms of the scattering phase shifts in a Fermi liquid description [93]. In turn, these phase shifts can be related to the expectation values $n_{\alpha\sigma} = \langle d^\dagger_{\alpha\sigma} d_{\alpha\sigma}\rangle$ of the even and odd states generalizing the Friedel sum rule to the SU(4) model with a symmetry breaking field (see Appendix C of Ref. [73])

$$G_0 = \frac{e^2}{h}\sum_\sigma \sin^2[\pi(n_{e\sigma} - n_{o\sigma})], \quad (14)$$

and $n_{e\sigma} - n_{o\sigma}$ is linear in δ [57]. This is expected since in the SU(4) limit, the effect of δ and magnetic field are the same interchanging orbital and spin indices. Therefore, for small enough T, the conductance is proportional to δ^2. In contrast the thermal current is finite for $\delta = t = 0$ due to the effect of U'. This fact is known from previous calculations in a spinless model [38,39,94–96]. A simple physical explanation of this effect is provided in Ref. [39]. At low energies the effective interaction between the quasiparticles are renormalized, but the interdot repulsion remains significant [57].

In Fig. 4 we show the behavior of the Seebeck coefficient S, for several values of δ_4. In the SU(4) regime of small δ_4, S behaves similarly as the corresponding SU(4) result without destructive interference [20]. At low temperatures, the thermopower is dominated by the Kondo peak in the spectral density al low energies which lies above the Fermi energy, thus, it is negative, characteristic of hole transport. Instead at temperatures of the order of the charge-transfer energy $|E_d|$, S is dominated by the charge transfer peak, which is centered at E_d and is below the Fermi energy. Therefore, S changes sign at intermediate temperatures. However, while the maximum

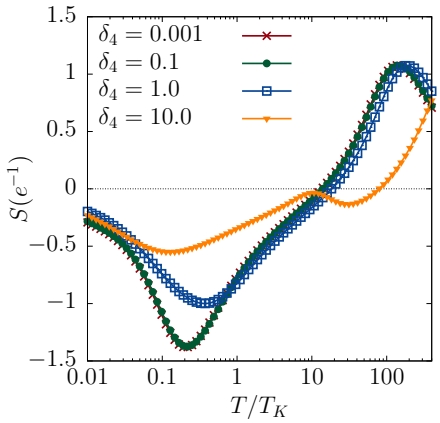

FIG. 4. Thermopower as a function of temperature for several values of δ_4.

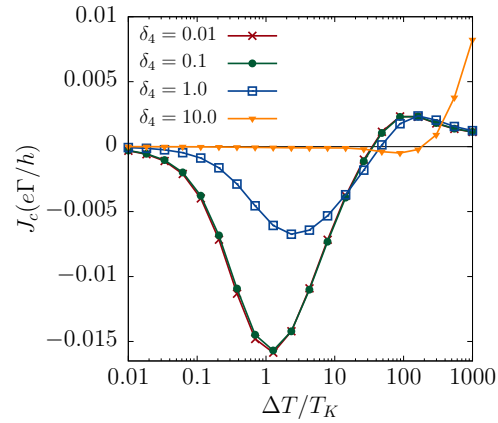

FIG. 6. Electrical current as a function of the temperature difference $\Delta T = T_L - T_R$, keeping $T_R = 0.1T_K$. For clarity, curves are rescaled with factors: 10^6, 10^2, and 10 for $\delta_4 = 0.01$, 0.1 and 10, respectively.

value of $|S|$ in the standard SU(4) case is near 1 k_B/Γ, in our case with destructive interference it is about 40% larger.

Increasing δ_4, the low-energy minimum approaches zero because the Kondo peak moves towards the Fermi energy. One also expects a negative contribution at energies of the order of δ due to the peak at energy δ in the spectral density of the odd state, which competes with the positive contribution of the charge transfer peaks at energies E_d and $E_d + \delta$ below the Fermi energy.

In Fig. 5 we show the figure of merit, which can be relevant for possible applications [1,97]. One can see that the most convenient choice to increase ZT is the intermediate regime $\delta_4 \sim 1$, where ZT can reach 1/4.

In Fig. 6 we show the thermoelectric current induced by a difference in the temperature between the left and right leads $\Delta T = T_L - T_R$. In spite of the obviously different physical situation, the curve has some features that resemble the thermopower shown above. For small δ_4 and ΔT, negatively charged electrons are excited in the Kondo peak above the Fermi level at the left dot and move to the right, originating a positive particle current and a negative charge current. When the left lead reaches temperatures of the order of the charge transfer peak $|E_d|$, holes are promoted in this lead which can be filled from electrons of the right lead, leading to negative particle current and positive charge current.

Similar arguments can be followed for large δ_4 [in the SU(2) regime], following a reasoning analogous to that made above for the thermopower. However, in this case, the effect of increasing δ_4 seem more dramatic.

In Fig. 7 we represent the corresponding heat current for the same situation as the previous figure. It seems to reach important values only at energies near the charge-transfer energy $|E_d|$ and particularly for small δ_4.

B. Fluctuations between 1 and 2 particles in the system

The problem for fluctuations between 2 and 3 particles can be mapped into the corresponding one for 1 and 2 particles using the electron-hole transformation mentioned at the beginning of Sec. III A. In the following we refer to the latter case.

The configuration with two particles consists of a singlet even under inversion and an odd triplet separated by an energy difference which is small for large U, $E_0 = E_1 - J$

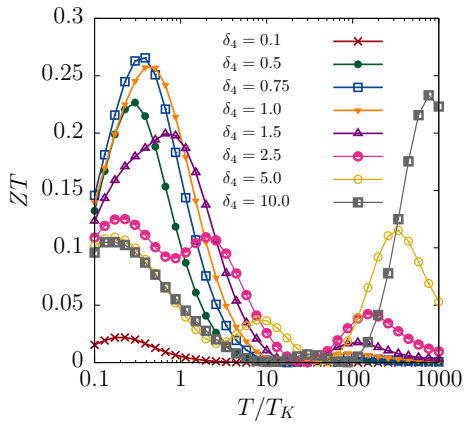

FIG. 5. Figure of merit as a function of temperature.

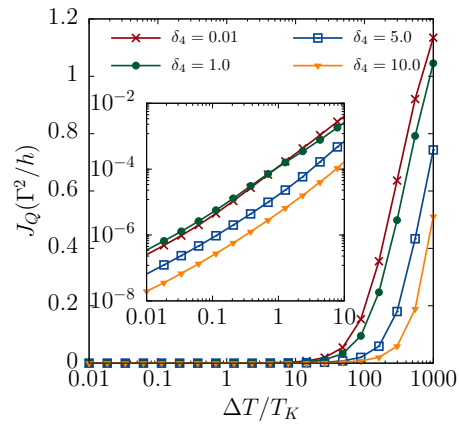

FIG. 7. Heat current as a function of the temperature difference $\Delta T = T_L - T_R$, keeping $T_R = 0.1T_K$. (Inset) Zoom of the region with $\Delta T/T_K$ lower than 10.

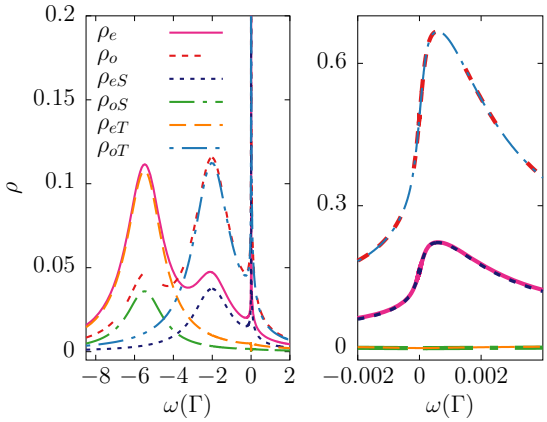

FIG. 8. Contribution of the two-particle singlet and triplet states to the spectral density of the even and odd states for $t = 1.5$, $U' = \chi = 0$ and $T = 10^{-4}$. Right panel: zoom of the region of the Kondo peak.

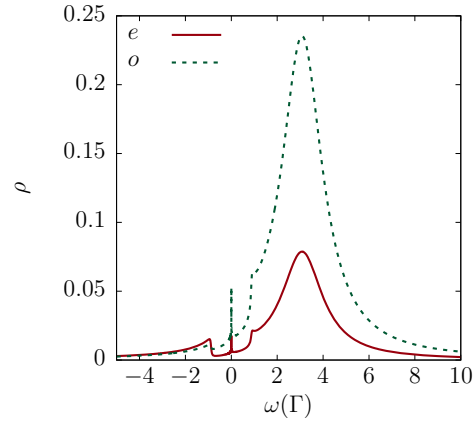

FIG. 9. Spectral density of the even and odd states for $t = 0.5$, $U' = 6$ and $T = 10^{-4}$.

with $J = 4t^2/(U - U')$. The configuration with one particle consists of an even doublet and an odd one. The two-particle configuration is that of lowest energy for small t and U'.

A model in which a singlet and a triplet are mixed with a doublet, all with the same parity has been studied first in the context of Tm impurities in a cubic crystal field [98] and more recently to explain experiments [99] in a single-molecule quantum dot [68–70], This model has a quantum phase transition (QPT) which separates two regions with a doublet or a singlet ground state. This transition is accurately described by the NRG [98]. With the NCA a change in the spectral density near the Fermi level, accompanied by a change in the occupancy of the triplet and singlet auxiliary bosons is found [69].

In the case of two dots interacting via a Heisenberg interaction, there is also a QPT which turns to a crossover when hopping between the dots is included [62,100]. It is likely that this QPT is related to the previous one.

In our model we find that for $\chi = 0$ (degeneracy of singlet and triplet states of the two-particle localized configuration) the triplet boson dominates, but small values of χ (of the order of 0.001) induce a crossover to the dominance of the singlet boson at low temperatures and the disappearance of the Kondo peak at the Fermi level.

As a basis for our study we take $\Gamma_L = \Gamma_R = 1$ as the unit of energy and $E_d = -3.5$. We also take for the moment $\chi = 0$. As before we choose the origin of one-particle energies at the Fermi level $\epsilon_F = 0$.

With the above assumptions, the energies for the even and odd one-particle states are $E_e = E_d - t$, $E_o = E_d + t$. The spectral density of these states is shown in Fig. 8 for a typical case in the regime of small t and U'. The Kondo peak lies slightly above the Fermi energy and the charge transfer peak is split by t. The even (odd) state has larger weight at $E_d - t$ ($E_d + t$). This is explained as follows. The ground state is composed mainly of the odd triplet with an even and an odd particle and total energy near $2E_d$. Destroying the even particle leaves the odd one with energy $E_d + t$. Therefore, the energy difference is $E_d - t$. Interchanging even and odd states the reasoning is similar with a change in the sign in front of t. Due to the even parity of the two-particle singlet, the contribution of this singlet to the split peaks is inverted with respect to the contribution of the triplets, which is the dominant one. Except for the splitting, the spectral density is qualitative similar to that expected for the ordinary Anderson model at large U.

When t reaches $|E_d|$, there is a change of valence and the one-particle even state becomes the ground state. The same happens with increasing U'. An example for the spectral density for large U' is shown in Fig. 9. It has three main features: the charge transfer peak, now at positive energies with respect to the Fermi level, approximately at $E_d + U' + t$ (which is the difference in energy between the two-particle states at $2E_d + U'$ and the ground one-particle state at $E_d - t$), a narrow Kondo peak at the Fermi energy (very slightly displaced to negative energies) and two inelastic features at $\pm 2t$ related to higher order processes involving transitions between even and odd one-particle states.

To study the behavior of different quantities, it is useful to define the energy scale related to the half width at half maximum of the Kondo peak, which is one way to define the Kondo temperature T_K. However, we had found that the result of fitting this resonance at the Fermi level depends on the range of the fit and it can vary within a factor 2 depending on this range [101]. Therefore, to determine T_K we have used the "pseudoconductance" $G_p(T)$, which is the conductance through one quantum dot with the total spectral density of our system, obtaining T_K from the expression $G_p(T_K) = G_p(0)/2$. In Fig. 10 we represent T_K obtained in this way as a function of U' in a logarithmic scale. In agreement with previous calculations using NRG [102], the energy scale increases strongly at the intermediate valence regime and decreases in going to the integer valence limits of two particles in the system for small U' or 1 particle for large U'.

The temperature dependence of the real conductance $G(T)$ through the system is shown in Fig. 11 in the regime of total occupancy near 2 in the system. For $t \gtrsim 0.5$, $G(T_K) \sim G(0)/2$ indicating that the conductance is dominated by the total density of states, as expected in general. However, for low t the behavior is dominated by the destructive interference. Not

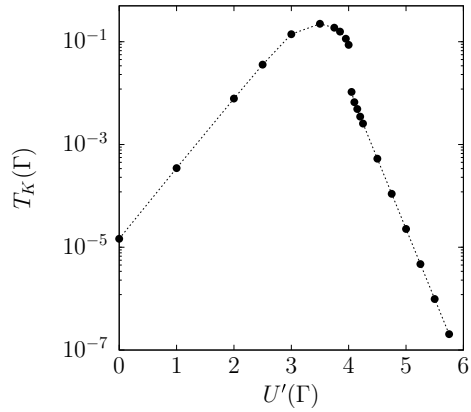

FIG. 10. Energy scale T_K obtained from the pseudoconductance (see text) as a function of U' for $t = 0$.

only $G(T) \to 0$ for $t \to 0$, but also a new small energy scale T^* appears which determines the temperature at which $G(T)$ begins to fall with increasing T. For $t \sim 10^{-2}$, $T^* \sim 10^{-2}T_K$.

In Fig. 12 we represent the thermal conductance κ as a function of temperature for the same parameters as in Fig. 11. It increases monotonically with T until temperatures greater than the charge-transfer energy are overcome. It is also clear that κ increases substantially as the intermediate-valence regime between total occupancies 2 and 1 is approached.

The thermal conductance for relatively large $U' = 6$, for which the occupancy of the system is slightly above 1, is shown in Fig. 13. There is a maximum at temperatures of the order of the charge-transfer energy. As expected, κ increases with increasing t, but the effect is not linear in t. Note that in contrast to the previous figures, there is a significant thermal conductance at $t = 0$ due to the effect of U'. This fact is known from previous calculations in a spinless model [38,39,94–96].

In Fig. 14 top panel, we show the thermopower as a function of temperature in the regime of total occupancy near 2. Since the spectral density is qualitatively similar to that of Sec. III A in the SU(4) regime, the figure has same features in common with Fig. 4. In particular, there is a dip at low temperatures due to the Kondo peak slightly above the Fermi

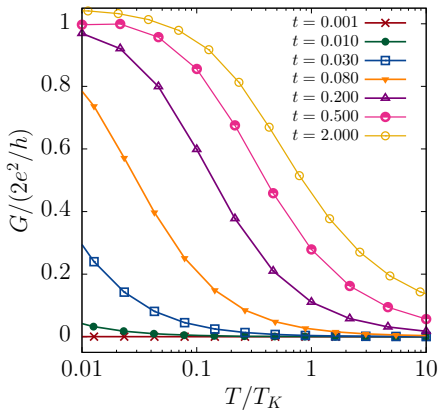

FIG. 11. Electrical conductance as a function of temperature for $U' = 0$ and several values of t.

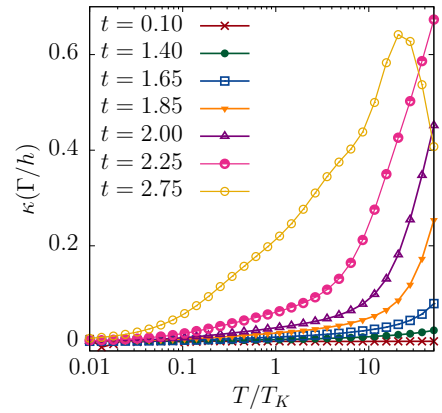

FIG. 12. Thermal conductance as a function of temperature for $U' = 0$ and several values of t.

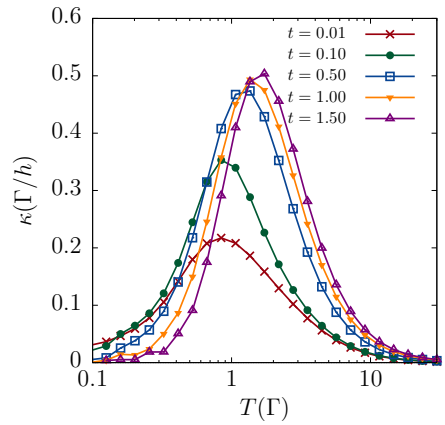

FIG. 13. Thermal conductance as a function of temperature for $U' = 6$ and several values of t.

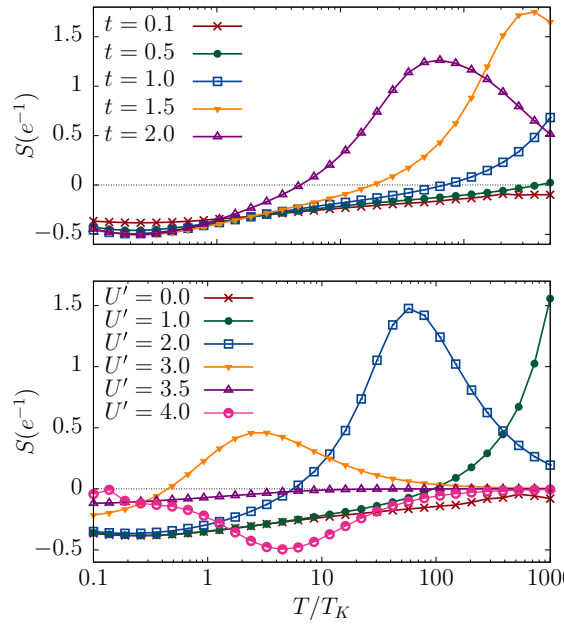

FIG. 14. Thermopower as a function of temperature. Top panel: for $U' = 0$ and several values of t. Bottom panel: for $t = 0.1$ and several values of U'.

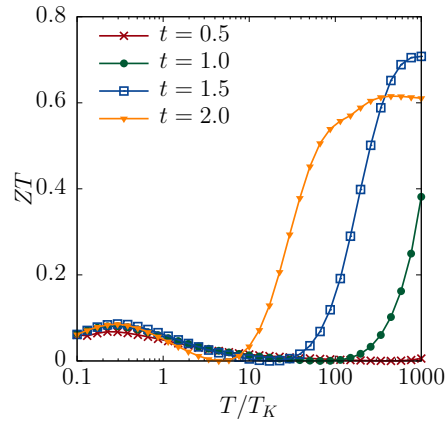

FIG. 15. Figure of merit as a function of temperature for $U' = 0$ and several values of t.

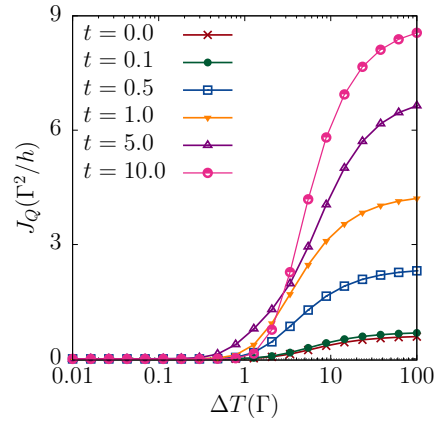

FIG. 17. Heat current as a function of the temperature difference $\Delta T = T_L - T_R$, keeping $T_R = 10^{-3}$ for $U' = 0$ and several values of t.

level and a peak at the charge-transfer energy $|E_d| - t$ due to the charge-transfer peak in the spectral density next to the Fermi level. The negative interference for $t \to 0$ tends to suppress both, the thermal and electrical conductances but does not affect the thermopower in a marked way.

In Fig. 14 bottom panel, we show the thermopower as a function of temperature for several values of U'. The peak at the temperature corresponding to the charge-transfer energy $\sim|E_d| - U'$ displaces to lower temperature with increasing U'. Entering the regime of total occupancy 1, for large U', the thermopower is strongly reduced, particularly at small temperatures, because the Kondo peak is nearly symmetric and with small intensity (see Fig. 9). In addition since now the charge-transfer peak in the spectral density lies at positive energies, the corresponding feature in the thermopower becomes negative.

The figure of merit ZT reaches values near 0.7 for temperatures of the order of the charge gap and $t \sim 1.5$, see Fig. 15.

The thermoelectric current, shown in Fig. 16 has qualitative features similar to the thermopower shown in Fig. 14 for small t. In particular, since there is a charge transfer peak below the Fermi level, at temperatures at which holes are excited in the

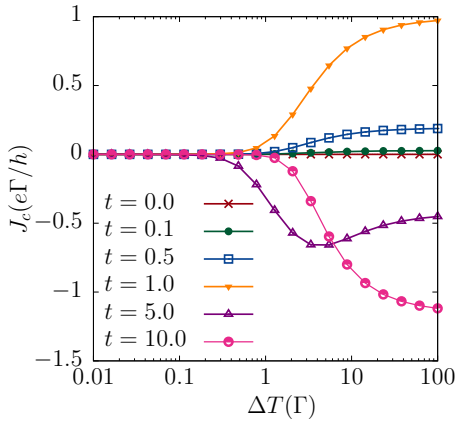

FIG. 16. Electrical current as a function of the temperature difference $\Delta T = T_L - T_R$, keeping $T_R = 10^{-3}$ for $U' = 0$ and several values of t.

left lead, these holes can move to the right lead leading to a positive charge current. However for $t > |E_d|$ there is a valence crossover from occupancy near 2 to 1 in the system, and the charge transfer peak moves above the Fermi level, leading to a change in the sign of the electrical current. Increasing U' has a similar effect (not shown).

In Fig. 17 we display the heat current for similar parameters as the previous figure. A noticeable effect is that even for $t = 0$, for a difference of temperature ΔT higher than Γ, there is a small but significant heat current due to the effect of correlations. Previous works have demonstrated this effect as a consequence of U' in a spinless model [38,39,94–96]. Here we obtain that a similar effect takes place also as a consequence of large on-site repulsion U, although our results for the thermal conductance (Fig. 12) give negligible values for $t = U' = 0$. We return to this point later, when the width of the spectral density of both dots is discussed (Fig. 18). The heat current increases as the occupancy is reduced from 2 to 1 at high temperatures.

When U' is included, as expected from previous work [39], the heat transport at $t = 0$ is larger in the intermediate valence regime, reaching values near $J_Q = 0.7(\Gamma^2/h)$ for $U' = 4$ and fixed $\Delta T = 10$. For $U' = 0$, J_Q is slightly below $0.2(\Gamma^2/h)$ For the sake of brevity we do not include here our studies for finite U'. As in previous studies [38,39,94–96], the heat current is large for $U' \neq 0$ even at $t = 0$. Instead, slave boson approaches give always $J_Q = 0$ for $t = 0$.

In contrast to Sierra *et al.* [36], we do not find a regime of decreasing J_Q with increasing ΔT. A discussion of the possible reasons for this discrepancy is left to Sec. IV.

As in the case of fluctuations between 0 and 1 particles presented in Sec. III A, we also find strong violations of the Wiedemann-Franz law. The ratio $J_Q/(TJ_c)$ ranges from $\sim 0.1/e^2$ for $\Delta T = 100$ to $\to \infty$ for parameters for which $J_c \to 0$ (not shown).

In Fig. 18 we show the evolution of the widths of the spectral densities at both dots as a function of the temperature of the left (hot) lead T_L keeping the temperature of the right (cold) lead T_R constant. For the physical discussion below, we also show the result of the equilibrium situation, when the temperature of both leads is increased simultaneously

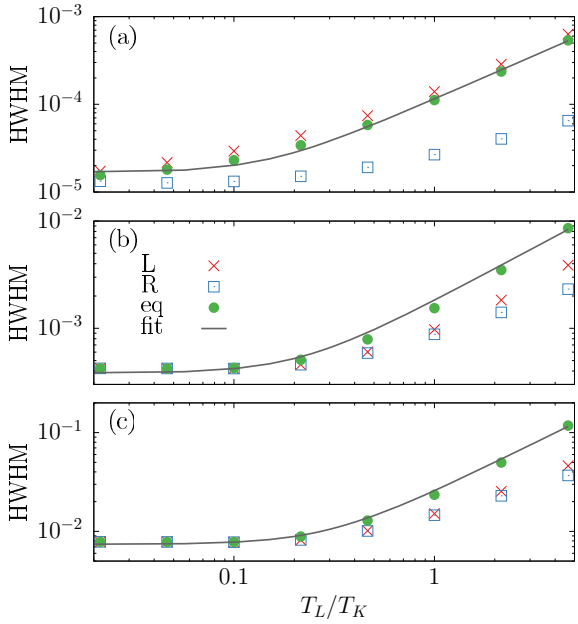

FIG. 18. half widths at half maximum of the spectral densities of the left (crosses) and right (squares) dots as a function of T_L, keeping $T_R = 0.01T_K$ for $U' = 0$ and (a) $t = 0.0$, (b) $t = 1.0$ and (c) $t = 1.85$. The green dots correspond to both leads at temperature T_L.

($T_R = T_L$ instead of fixed T_R). In this case, the half width at half maximum (HWHM) of the spectral density is expected to vary with temperature according to

$$\text{HWHM} = \sqrt{(\alpha T)^2 + T_K^2}, \tag{15}$$

where α is fitting parameter [72,103]. As it happened previously [72], the NCA results are well fitted by this expression (full lines in Fig. 18), with values of α in the range between 3 and 8, similar to values previously obtained [72,103].

For $t = 0$ both dots are disconnected by the one-particle terms of the Hamiltonian. One would expect then that each dot reaches the temperature of the corresponding lead in the absence of interatomic interactions ($U' = 0$). The HWHM of the left dot is slightly above the equilibrium value at temperature T_L. Except for this small deviation, the result agrees with the expectations. Instead, one would expect that the HWHM of the right dot remains at the corresponding value for T_R. However, it increases moderately with increasing T_L. One knows that in presence of interatomic interactions, in particular U', there is heat transfer between the dots [38,39,94–96], and this is consistent with the different results presented here. However, it is not obvious that a similar effect can exist for $U' = 0$. A plausible explanation is that U' is generated at low energies. In fact previous calculations show that even if the bare U' is small, the renormalized low-energy parameter is of the same order of magnitude as the renormalized intradot repulsions (see Fig. 7 of Ref. [57]).

As t increases, one expects an interchange of heat between the dots and that the HWHMs are intermediate between those corresponding to the equilibrium ones, replacing T by either T_L or T_R in Eq. (15). This is indeed what happens. For large

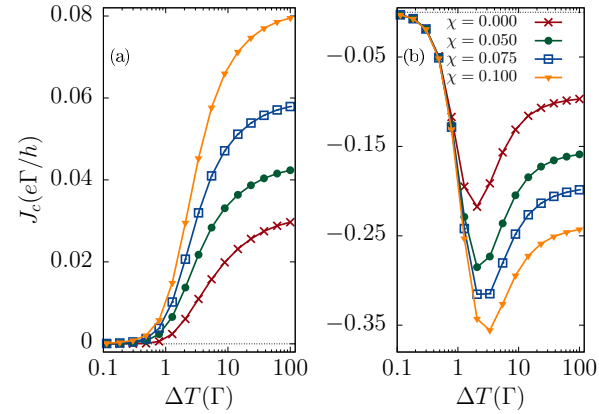

FIG. 19. Electrical current as a function of the temperature difference $\Delta T = T_L - T_R$, keeping $T_R = 0.1T_K$ for $t = 0.1$, different values of χ and (a) $U' = 0$ and (b) $U' = 6$.

hopping, the results of Fig. 18 indicate that both dots tend to be at the same temperature, intermediate to those of both leads.

Effect of triplet-singlet splitting

In this section, we examine the effect of a finite triplet-singlet splitting on the thermoelectric properties out of equilibrium.

The effect of a finite triplet-singlet splitting on the electrical current produced by a finite temperature difference between the leads is shown in Fig. 19(a). The thermoelectric current is enhanced at moderate temperatures. The same happens at large U'. However, in this case since the charge-transfer peak is above the Fermi energy, electrons flow from the cold to the hot lead, leading to a negative particle current and a positive charge current. The heat current is also enhanced.

IV. SUMMARY AND DISCUSSION

In summary, we have studied an inversion symmetric DQD system in series, with each dot connected to its own lead, under a thermal bias. We have used the noncrossing approximation in the limit of very large on-site Coulomb repulsion. In this limit, the problem can be divided into fluctuations between 0 and 1 electron (regime I) in the DQD, or between 1 and 2 electrons (regime 2). Other fillings are related to the previous ones by electron-hole symmetry.

The behavior of the different quantities studied can be understood from the energy dependence of the total spectral density $\rho(\omega)$ at equilibrium and low temperatures. While the charge conductance decreases in general with increasing temperature, the thermal conductance is maximum at temperatures of the order of the charge-transfer energy (the difference between the energies of the configurations with integer number of particles in the DQD). For interdot hopping $t = 0$, the heat conductance is negligible if the interdot repulsion U' is also zero, but increases significantly for finite U'. This fact is known from previous calculations in simplified systems [38,39,94–96], but is not reproduced by the simplest

SBMFA, because in the latter, the low-energy physics is reduced to an effective noninteracting system and the effect of U' is not included.

In contrast to previous work [36], we do not find regions of negative differential thermal conductance. The reason of the discrepancy is the following. As explained in Ref. [36], within the SBMFA the effective Kondo temperature of the hot lead is decreased with increasing temperature of the lead, and for very large temperatures the transport through the double dot is blocked. Therefore, the thermal transport is inhibited as the temperature of the hot lead is increased. We believe that this an artifact of the SBMFA, of similar character as the artificial decoupling of the impurity with increasing temperature [47] or magnetic field [82] found previously. Instead, the NCA actually improves with increasing temperature and the width of the spectral density follows the expected temperature dependence given by Eq. (15) (see Fig. 18 and Ref. [72]).

The sign of the charge current and the thermopower can be inferred from the positions and magnitude of the different peaks in $\rho(\omega)$, one related to the Kondo effect, near the Fermi energy and one or two related with charge-transfer processes, which can be above or below the Fermi energy. We find sign reversals of the thermoelectric current, in agreement with previous work [36]. In regime I, for small interdot hopping t, the thermopower S reaches a maximum absolute value at temperatures T below the Kondo energy scale T_K near $1.5/e$ and the Lorentz ratio diverges for $t \to 0$, indicating a strong violation of the Wiedemann-Franz law, unexpected from measurements in a large number of systems [87]. Previous deviations of this law calculated in mesoscopic systems were much more moderate [15,27]. There is also a maximum of S near 1 at high temperatures. This value is much higher than the corresponding one for a single-level quantum dot [17,20]. The figure of merit ZT reaches values of the order of 0.25 at $T \sim T_K$ for moderate t and at temperatures of the order of $2t$ for high t.

In regime II the thermopower reaches also high values but at temperatures of the order of the charge-transfer energy. The Lorentz ratio can be also very large or very small depending on the values of the parameters. On the other hand, $ZT \sim 0.7$ at high temperatures.

A study of the width of the nonequilibrium spectral densities of both dots, indicates that for small interdot hopping t, each dot is at the same temperature as the corresponding lead. Increasing t, the effective temperatures of both dots are intermediate between those of the leads and tend to coincide for t larger than the resonant level width Γ.

In this work, we have assumed inversion symmetry. This means that the on-site energy of both dots and coupling to the leads are the same. Asymmetric coupling to the leads can lead to a sizable enhancement of the thermoelectric response [28,31]. In addition, different energies of the dot can lead to important rectification effects [39]. It would be interesting to study these asymmetry effects.

ACKNOWLEDGMENT

A.A.A. acknowledges financial support provided by PICT 2017-2726 and PICT 2018-01546 of the ANPCyT, Argentina.

TABLE I. Matrix elements $D_{\nu\sigma}^{Sm,\xi\sigma'}$ entering Eq. (8) to linear order in $\chi = t/(U - U')$ for $\nu = R$ and $\sigma = \uparrow$.

$D_{R\uparrow}^{Sm,\xi\sigma'}$	$e\uparrow$	$o\uparrow$	$e\downarrow$	$o\downarrow$
1, 1	$\frac{-1}{\sqrt{2}}$	$\frac{-1}{\sqrt{2}}$	0	0
1, 0	0	0	$-\frac{1}{2}$	$-\frac{1}{2}$
1, −1	0	0	0	0
0, 0	0	0	$\frac{1}{2}+\chi$	$\frac{1}{2}-\chi$

APPENDIX A: NONCROSSING APPROXIMATION TREATMENT OF FLUCTUATIONS BETWEEN 1 AND 2 PARTICLES IN THE DQD

In this Appendix we describe in some detail the NCA approximation of the serial DQD attached to two different conducting leads as given by Eqs. (7) and (8). Performing the explicit calculations, the matrix elements $D_{\nu\sigma}^{Sm,\xi\sigma'} = \langle S, m|d_{\nu\sigma}^\dagger|\xi\sigma'\rangle$ entering Eq. (8) to linear order in $\chi = t/(U - U')$ turn out to be those displayed in Tables I to IV.

Auxiliary particle representation. Now, we introduce auxiliary bosons and fermions to represent the two-electron and one-electron states, $|S, m\rangle \to b_{S,m}^\dagger|vac\rangle$ and $|\xi\sigma\rangle \to f_{\xi\sigma}^\dagger|vac\rangle$, respectively, where $|vac\rangle$ is a reference state in the auxiliary Fock space. By using this representation the Hamiltonian in Eq. (7) reads as follows:

$$H_{eff} = \sum_{\xi\sigma} E_\xi f_{\xi\sigma}^\dagger f_{\xi\sigma} + \sum_{Sm} E_S b_{S,m}^\dagger b_{S,m} + H_c + H_V, \quad \text{(A1)}$$

where the hybridization term becomes

$$H_V = \sum_{k\nu\sigma}\sum_{\xi\sigma'}\sum_{Sm} V_{k\nu}\, D_{\nu\sigma}^{Sm,\xi\sigma'} b_{S,m}^\dagger f_{\xi\sigma'} c_{\nu k\sigma} + \text{H.c.} \quad \text{(A2)}$$

The auxiliary particles satisfy the constraint $\sum_{\xi\sigma} f_{\xi\sigma}^\dagger f_{\xi\sigma} + \sum_{Sm} b_{S,m}^\dagger b_{S,m} = 1$, which represents the completeness relation of the Hilbert space formed by the states in Eqs. (6). Furthermore, the expression of the physical creation operator at each dot is given by

$$d_{\nu\sigma}^\dagger = \sum_{\xi\sigma'}\sum_{Sm} D_{\nu\sigma}^{Sm,\xi\sigma'} b_{S,m}^\dagger f_{\xi\sigma'}. \quad \text{(A3)}$$

In this form, the Hamiltonian is suitable for the NCA treatment.

TABLE II. Matrix elements $D_{\nu\sigma}^{Sm,\xi\sigma'}$ entering Eq. (8) to linear order in $\chi = t/(U - U')$ for $\nu = L$ and $\sigma = \uparrow$.

$D_{L\uparrow}^{Sm,\xi\sigma'}$	$e\uparrow$	$o\uparrow$	$e\downarrow$	$o\downarrow$
1, 1	$\frac{1}{\sqrt{2}}$	$\frac{-1}{\sqrt{2}}$	0	0
1, 0	0	0	$\frac{1}{2}$	$-\frac{1}{2}$
1, −1	0	0	0	0
0, 0	0	0	$\frac{1}{2}+\chi$	$-\frac{1}{2}+\chi$

TABLE III. Matrix elements $D_{\nu\sigma}^{Sm,\xi\sigma'}$ entering Eq. (8) to linear order in $\chi = t/(U-U')$ for $\nu = R$ and $\sigma = \downarrow$.

$D_{R\downarrow}^{Sm,\xi\sigma'}$	$e\uparrow$	$o\uparrow$	$e\downarrow$	$o\downarrow$
1, 1	0	0	0	0
1, 0	$-\frac{1}{2}$	$-\frac{1}{2}$	0	0
1, −1	0	0	$\frac{-1}{\sqrt{2}}$	$\frac{-1}{\sqrt{2}}$
0, 0	$-\frac{1}{2}-\chi$	$-\frac{1}{2}+\chi$	0	0

Noncrossing Approximation. Starting from the auxiliary Green functions in the time domain,

$$\begin{aligned} G^{>}_{\xi\sigma,\xi'\sigma'}(t) &= -i\langle f_{\xi\sigma}(t) f^{\dagger}_{\xi'\sigma'}(0)\rangle, \\ G^{<}_{\xi\sigma,\xi'\sigma'}(t) &= +i\langle f^{\dagger}_{\xi'\sigma'}(0) f_{\xi\sigma}(t)\rangle, \\ B^{>}_{Sm}(t) &= -i\langle b_{S,m}(t) b^{\dagger}_{S,m}(0)\rangle, \\ B^{<}_{Sm}(t) &= -i\langle b^{\dagger}_{S,m}(0) b_{S,m}(t)\rangle, \end{aligned} \tag{A4}$$

and from Eq. (A1) we can write down the auxiliary selfenergies for the auxiliary particles as follows:

$$\begin{aligned} \Sigma^{\gtrless}_{\xi\sigma',\xi'\sigma''}(\omega) &= \pm \sum_{\nu\sigma,Sm_S} \Gamma_{\nu\sigma} D^{Sm_S,\xi\sigma'}_{\nu\sigma} D^{\xi'\sigma'',Sm_S}_{\nu\sigma} \\ &\quad \times \int \frac{d\omega'}{2\pi} f_{\nu}(\pm\omega') B^{\gtrless}_{Sm_S}(\omega'+\omega+\mu_{\nu}) \\ \Pi^{\gtrless}_{Sm_S}(\omega) &= \pm \sum_{\nu\sigma,\xi\sigma',\xi'\sigma''} \Gamma_{\nu\sigma} D^{Sm_S,\xi\sigma'}_{\nu\sigma} D^{\xi'\sigma'',Sm_S}_{\nu\sigma} \\ &\quad \times \int \frac{d\omega'}{2\pi} f_{\nu}(\pm\omega') G^{\gtrless}_{\xi\sigma',\xi'\sigma''}(\omega'+\omega-\mu_{\nu}), \end{aligned} \tag{A5}$$

where $f_{\nu}(\omega) = [1+e^{\omega/T_{\nu}}]^{-1}$ is the Fermi function at temperature T_{ν}.

The complete set of lesser and greater self-energies are purely imaginary functions. Therefore, the imaginary part of the retarded self-energies are given by

$$\begin{aligned} \mathrm{Im}\,\Sigma^{r}_{\xi\xi',\sigma}(\omega) &= \Sigma^{>}_{\xi\xi',\sigma}(\omega)/2, \\ \mathrm{Im}\,\Pi^{r}_{Sm_S}(\omega) &= \Pi^{>}_{Sm_S}(\omega)/2, \end{aligned} \tag{A6}$$

while the real parts can be obtained from the imaginary ones by using a Kramers-Kronig transformation.

In addition, $G^{\gtrless}_{\xi\xi} = i\mathbb{G}^{\gtrless}_{\xi\xi}$, $G^{\gtrless}_{\xi\xi'} + G^{\gtrless}_{\xi'\xi} = i(\mathbb{G}^{\gtrless}_{\xi\xi'} + \mathbb{G}^{\gtrless}_{\xi'\xi})$, with $\xi \neq \xi'$, and $B^{\gtrless} = i\mathbb{B}^{\gtrless}$ are purely imaginary. Regarding signs, $\mathbb{G}^{<}_{\xi\xi} > 0$ and $\mathbb{G}^{>}_{\xi\xi} < 0$ and $\mathbb{B}^{\gtrless} < 0$ (at least in equilibrium). The constraint, being a positive magnitude, reads $Q = \int \frac{d\omega}{2\pi} (\sum_{\xi,\sigma} \mathbb{G}^{<}_{\xi\xi,\sigma}(\omega) - \sum_{Sm_S} \mathbb{B}^{<}_{Sm_S}(\omega))$.

TABLE IV. Matrix elements $D_{\nu\sigma}^{Sm,\xi\sigma'}$ entering Eq. (8) to linear order in $\chi = t/(U-U')$ for $\nu = L$ and $\sigma = \downarrow$.

$D_{L\downarrow}^{Sm,\xi\sigma'}$	$e\uparrow$	$o\uparrow$	$e\downarrow$	$o\downarrow$
1, 1	0	0	0	0
1, 0	$\frac{1}{2}$	$-\frac{1}{2}$	0	0
1, −1	0	0	$\frac{1}{\sqrt{2}}$	$\frac{-1}{\sqrt{2}}$
0, 0	$-\frac{1}{2}-\chi$	$\frac{1}{2}-\chi$	0	0

For the fermion retarded Green functions we obtain

$$\begin{aligned} G^{r}_{ee,\sigma}(\omega) &= (\omega - E_o - \Sigma^{r}_{oo,\sigma}(\omega))/\mathbb{D}(\omega), \\ G^{r}_{oo,\sigma}(\omega) &= (\omega - E_e - \Sigma^{r}_{ee,\sigma}(\omega))/\mathbb{D}(\omega), \\ G^{r}_{eo,\sigma}(\omega) &= \Sigma^{r}_{eo,\sigma}(\omega)/\mathbb{D}(\omega),\ G^{r}_{oe,\sigma}(\omega) = \Sigma^{r}_{oe,\sigma}(\omega)/\mathbb{D}(\omega), \\ \mathbb{D}(\omega) &= (\omega - E_o - \Sigma^{r}_{oo,\sigma}(\omega))(\omega - E_e - \Sigma^{r}_{ee,\sigma}(\omega)) \\ &\quad - \Sigma^{r}_{eo,\sigma}(\omega)\Sigma^{r}_{oe,\sigma}(\omega). \end{aligned} \tag{A7}$$

On the other hand, the bosons retarded Green functions read as follows:

$$B^{r}_{Sm_S}(\omega) = \frac{1}{\omega - E_S - \Pi^{r}_{Sm_S}(\omega)}. \tag{A8}$$

The self-consistent procedure closes with the matrix relations

$$G^{\gtrless} = G^{r}\Sigma^{\gtrless}G^{a}, \quad B^{\gtrless} = B^{r}\Pi^{\gtrless}B^{a}. \tag{A9}$$

An example for a particular matrix element is

$$G^{>}_{eo} = \sum_{\mu\nu} G^{r}_{e\mu}\Sigma^{>}_{\mu\nu}G^{a}_{\nu o}. \tag{A10}$$

Physical Green functions. By using the auxiliary expression of the physical operator in Eq. (A3) the physical Green functions for each dot are given by

$$\begin{aligned} G^{\gtrless}_{\nu\nu',\sigma}(\omega) &= -\frac{i}{Q}\sum_{\xi\xi'\sigma'}\sum_{Sm_S} D^{\xi\sigma',Sm_S}_{\nu\sigma} D^{Sm_S,\xi'\sigma'}_{\nu'\sigma} \\ &\quad \times \int \frac{d\omega'}{2\pi} G^{\lessgtr}_{\xi\xi',\sigma'}(\omega') B^{\gtrless}_{Sm_S}(\omega'+\omega). \end{aligned} \tag{A11}$$

APPENDIX B: AN ALTERNATIVE EXPRESSION FOR THE CHARGE CURRENT

In this Appendix we give an alternative expression for the calculation of the charge current for the Hamiltonian Eqs. (1) to (4) of the main text. Current conservation along the system leads to the following relation:

$$\frac{d}{dt}(N_L + n_L) = -\frac{d}{dt}(N_R + n_R), \tag{B1}$$

where $n_i = \sum_{\sigma} n_{i\sigma}$ and $N_i = \sum_{k_i\sigma} c^{\dagger}_{k_i\sigma} c_{k_i\sigma}$. Therefore, the electric current can be computed from the left part of the system by using the Heisenberg equation of motion

$$\hat{J}^{C}_{L} \equiv \frac{e}{\hbar}\frac{d}{dt}(N_L + n_L) = -i\frac{e}{\hbar}[N_L + n_L, H]. \tag{B2}$$

After some algebra and by using the identity $[n_{i\sigma}, n_{j\sigma'}] = -\delta_{ij}\delta_{\sigma\sigma'}(c^{\dagger}_{j\sigma'}c_{i\sigma} + c^{\dagger}_{i\sigma}c_{j\sigma'})$ the right-hand side simplifies to

$$\hat{J}^{C}_{L} = -\frac{ie}{\hbar}t\sum_{\sigma}(d^{\dagger}_{R\sigma}d_{L\sigma} - d^{\dagger}_{L\sigma}d_{R\sigma}), \tag{B3}$$

which is nothing but the usual form of the current operator between two sites of a linear chain with a hopping equal to t. The Fourier transform $G^{<}_{ij,\sigma}(\omega)$ of the time-dependent Green's functions $G^{<}_{ij,\sigma}(t) = i\langle d^{\dagger}_{j\sigma} d_{i\sigma}(t)\rangle$ provides the average of $\hat{J}^{C}_{L}$

leading the expression for the current in the form

$$J_L^C = \frac{e}{\hbar} t \sum_\sigma \int \frac{d\omega}{2\pi} (G^<_{LR,\sigma}(\omega) - G^<_{RL,\sigma}(\omega)) = \frac{e}{\hbar} t \sum_\sigma \int \frac{d\omega}{2\pi} (G^<_{eo,\sigma}(\omega) - G^<_{oe,\sigma}(\omega)). \quad \text{(B4)}$$

Note that the last expression follows from $\langle d^\dagger_{R\sigma} d_{L\sigma} - d^\dagger_{L\sigma} d_{R\sigma} \rangle = \langle d^\dagger_{e\sigma} d_{o\sigma} - d^\dagger_{o\sigma} d_{e\sigma} \rangle$. Using that $G^<_{oe,\sigma}(\omega)$ is the complex conjugate of $G^<_{eo,\sigma}(\omega)$, being both purely imaginary, and adding both spins, one arrives at Eq. (12) of the main text.

[1] G. Benenti, G. Casati, K. Saito, and R. S. Whitney, Fundamental aspects of steady-state conversion of heat to work at the nanoscale, Phys. Rep. **694**, 1 (2017).

[2] S. Guo, G. Zhou, and N. Tao, Single molecule conductance, thermopower, and transition voltage, Nano Lett. **13**, 4326 (2013).

[3] D. Kim, P. S. Yoo, and T. Kim, Length-dependent thermopower determination of amine-terminated oligophenyl single molecular junctions formed with ag electrodes, J. Korean Phys. Soc. **66**, 602 (2015).

[4] L. Rincón-García, C. Evangeli, G. Rubio-Bollinger, and N. Agraït, Thermopower measurements in molecular junctions, Chem. Soc. Rev. **45**, 4285 (2016).

[5] L. Cui, R. Miao, C. Jiang, E. Meyhofer, and P. Reddy, Perspective: Thermal and thermoelectric transport in molecular junctions, J. Chem. Phys. **146**, 092201 (2017).

[6] R. Miao, H. Xu, M. Skripnik, L. Cui, K. Wang, K. G. L. Pedersen, M. Leijnse, F. Pauly, K. Wärnmark, E. Meyhofer, P. Reddy, and H. Linke, Influence of quantum interference on the thermoelectric properties of molecular junctions, Nano Lett. **18**, 5666 (2018).

[7] L. Cui, S. Hur, Z. A. Akbar, J. C. Klöckner, W. Jeong, F. Pauly, S.-Y. Jang, P. Reddy, and E. Meyhofer, Thermal conductance of single-molecule junctions, Nature (London) **572**, 628 (2019).

[8] P. A. Erdman, J. T. Peltonen, B. Bhandari, B. Dutta, H. Courtois, R. Fazio, F. Taddei, and J. P. Pekola, Nonlinear thermovoltage in a single-electron transistor, Phys. Rev. B **99**, 165405 (2019).

[9] A. Svilans, M. Josefsson, A. M. Burke, S. Fahlvik, C. Thelander, H. Linke, and M. Leijnse, Thermoelectric characterization of the Kondo resonance in nanowire quantum dots, Phys. Rev. Lett. **121**, 206801 (2018).

[10] M. Josefsson, A. Svilans, A. M. Burke, E. A. Hoffmann, S. Fahlvik, C. Thelander, M. Leijnse, and H. Linke, A quantum-dot heat engine operating close to the thermodynamic efficiency limits, Nat. Nanotechnol. **13**, 920 (2018).

[11] B. Dutta, D. Majidi, A. García Corral, P. A. Erdman, S. Florens, T. A. Costi, H. Courtois, and C. B. Winkelmann, Direct probe of the seebeck coefficient in a Kondo-correlated single-quantum-dot transistor, Nano Lett. **19**, 506 (2019).

[12] D. Boese and R. Fazio, Thermoelectric effects in kondo-correlated quantum dots, Europhys. Lett. **56**, 576 (2001).

[13] T. E. Humphrey, R. Newbury, R. P. Taylor, and H. Linke, Reversible quantum Brownian heat engines for electrons, Phys. Rev. Lett. **89**, 116801 (2002).

[14] M. Krawiec and K. I. Wysokiński, Thermoelectric phenomena in a quantum dot asymmetrically coupled to external leads, Phys. Rev. B **75**, 155330 (2007).

[15] B. Kubala, J. König, and J. Pekola, Violation of the Wiedemann-Franz law in a single-electron transistor, Phys. Rev. Lett. **100**, 066801 (2008).

[16] R. Świrkowicz, M. Wierzbicki, and J. Barnaś, Thermoelectric effects in transport through quantum dots attached to ferromagnetic leads with noncollinear magnetic moments, Phys. Rev. B **80**, 195409 (2009).

[17] T. A. Costi and V. Zlatić, Thermoelectric transport through strongly correlated quantum dots, Phys. Rev. B **81**, 235127 (2010).

[18] M. Leijnse, M. R. Wegewijs, and K. Flensberg, Nonlinear thermoelectric properties of molecular junctions with vibrational coupling, Phys. Rev. B **82**, 045412 (2010).

[19] J. Azema, A.-M. Daré, S. Schäfer, and P. Lombardo, Kondo physics and orbital degeneracy interact to boost thermoelectrics on the nanoscale, Phys. Rev. B **86**, 075303 (2012).

[20] P. Roura-Bas, L. Tosi, A. A. Aligia, and P. S. Cornaglia, Thermopower of an SU(4) Kondo resonance under an SU(2) symmetry-breaking field, Phys. Rev. B **86**, 165106 (2012).

[21] A. A. Aligia, Nonequilibrium self-energies, Ng approach, and heat current of a nanodevice for small bias voltage and temperature, Phys. Rev. B **89**, 125405 (2014).

[22] J. Azema, P. Lombardo, and A.-M. Daré, Conditions for requiring nonlinear thermoelectric transport theory in nanodevices, Phys. Rev. B **90**, 205437 (2014).

[23] A. Dorda, M. Ganahl, S. Andergassen, W. von der Linden, and E. Arrigoni, Thermoelectric response of a correlated impurity in the nonequilibrium Kondo regime, Phys. Rev. B **94**, 245125 (2016).

[24] M. A. Sierra, R. López, and D. Sánchez, Fate of the spin-$\frac{1}{2}$ kondo effect in the presence of temperature gradients, Phys. Rev. B **96**, 085416 (2017).

[25] H. Li, Y. Wang, X. kang, S. Liu, and R. Li, Enhancement of thermoelectric properties in benzene molecule junction by the magnetic flux, J. Appl. Phys. **121**, 065105 (2017).

[26] Z. Li, Y. Cheng, JianHua Wei, X. Zheng, and YiJing Yan, Kondo-peak splitting and resonance enhancement caused by interdot tunneling in coupled double quantum dots, Phys. Rev. B **98**, 115133 (2018).

[27] M. Bürkle and Y. Asai, How to probe the limits of the WiedemannFranz law at nanoscale, Nano Lett. **18**, 7358 (2018).

[28] D. Pérez Daroca, P. Roura-Bas, and A. A. Aligia, Enhancing the nonlinear thermoelectric response of a correlated quantum dot in the Kondo regime by asymmetrical coupling to the leads, Phys. Rev. B **97**, 165433 (2018).

[29] D. B. Karki and M. N. Kiselev, Nonlinear seebeck effect of SU(n) kondo impurity, Phys. Rev. B **100**, 125426 (2019).

[30] L. Tesser, B. Bhandari, P. A. Erdman, E. Paladino, R. Fazio, and F. Taddei, Heat rectification through single and coupled quantum dots, New J. Phys. **24**, 035001 (2022).

[31] A. Manaparambil and I. Weymann, Nonequilibrium Seebeck effect and thermoelectric efficiency of Kondo-correlated molecular junctions, Phys. Rev. B **107**, 085404 (2023).

[32] E. L. Minarelli, J. B. Rigo, and A. K. Mitchell, Linear response quantum transport through interacting multi-orbital nanostructures, arXiv:2209.01208.

[33] R. S. Cortes-Santamaria, J. A. Landazabal-Rodríguez, J. Silva-Valencia, E. Ramos, M. S. Figueira, and R. Franco, Universality and the thermoelectric transport properties of a double quantum dot system: Seeking for conditions that improve the thermoelectric efficiency, arXiv:2302.09099.

[34] S. Donsa, S. Andergassen, and K. Held, Double quantum dot as a minimal thermoelectric generator, Phys. Rev. B **89**, 125103 (2014).

[35] G. T. Craven, D. He, and A. Nitzan, Electron-transfer-induced thermal and thermoelectric rectification, Phys. Rev. Lett. **121**, 247704 (2018).

[36] M. A. Sierra, R. López, and J. S. Lim, Thermally driven out-of-equilibrium two-impurity Kondo system, Phys. Rev. Lett. **121**, 096801 (2018).

[37] A.-M. Daré, Comparative study of heat-driven and power-driven refrigerators with Coulomb-coupled quantum dots, Phys. Rev. B **100**, 195427 (2019).

[38] H. K. Yadalam and U. Harbola, Statistics of heat transport across a capacitively coupled double quantum dot circuit, Phys. Rev. B **99**, 195449 (2019).

[39] A. A. Aligia, D. P. Daroca, L. Arrachea, and P. Roura-Bas, Heat current across a capacitively coupled double quantum dot, Phys. Rev. B **101**, 075417 (2020).

[40] M. Lavagna, V. Talbo, T. Q. Duong, and A. Crépieux, Level anticrossing effect in single-level or multilevel double quantum dots: Electrical conductance, zero-frequency charge susceptibility, and Seebeck coefficient, Phys. Rev. B **102**, 115112 (2020).

[41] P. Lombardo, R. Hayn, D. Zhuravel, and S. Schäfer, Kondo-assisted switching between three conduction states in capacitively coupled quantum dots, Phys. Rev. Res. **2**, 033387 (2020).

[42] Y. Zhang and S. Su, Thermal rectification and negative differential thermal conductance based on a parallel-coupled double quantum-dot, Physica A **584**, 126347 (2021).

[43] S. Ghosh, N. Gupt, and A. Ghosh, Universal behavior of the coulomb-coupled fermionic thermal diode, Entropy **24**, 1810 (2022).

[44] A. Manaparambil and W. I., Nonequilibrium seebeck effect and spin seebeck effects in nanoscale junctions, arXiv:2307.10393.

[45] F. B. Anders, Steady-state currents through nanodevices: A scattering-states numerical renormalization-group approach to open quantum systems, Phys. Rev. Lett. **101**, 066804 (2008).

[46] H. T. M. Nghiem and T. A. Costi, Time-dependent numerical renormalization group method for multiple quenches: Towards exact results for the long-time limit of thermodynamic observables and spectral functions, Phys. Rev. B **98**, 155107 (2018).

[47] A. C. Hewson, *The Kondo Problem to Heavy Fermions* (Cambridge University Press, Cambridge, 1997).

[48] M. A. Romero, S. C. Gómez-Carrillo, P. G. Bolcatto, and E. C. Goldberg, Spin fluctuation effects on the conductance through a single Pd atom contact, J. Phys.: Condens. Matter **21**, 215602 (2009).

[49] R. Van Roermund, Shiue-yuan Shiau, and M. Lavagna, Anderson model out of equilibrium: Decoherence effects in transport through a quantum dot, Phys. Rev. B **81**, 165115 (2010).

[50] M. A. Romero, F. Flores, and E. C. Goldberg, Effective treatment of charge and spin fluctuations in dynamical and static atom-surface interactions, Phys. Rev. B **80**, 235427 (2009).

[51] A. Crépieux, S. Sahoo, T. Q. Duong, R. Zamoum, and M. Lavagna, Emission noise in an interacting quantum dot: Role of inelastic scattering and asymmetric coupling to the reservoirs, Phys. Rev. Lett. **120**, 107702 (2018).

[52] A. Oguri, Fermi-liquid theory for the anderson model out of equilibrium, Phys. Rev. B **64**, 153305 (2001).

[53] A. Oguri and A. C. Hewson, Higher-order Fermi-liquid corrections for an Anderson impurity away from half filling: Nonequilibrium transport, Phys. Rev. B **97**, 035435 (2018).

[54] C. Mora, P. Vitushinsky, X. Leyronas, A. A. Clerk, and K. Le Hur, Theory of nonequilibrium transport in the SU(n) Kondo regime, Phys. Rev. B **80**, 155322 (2009).

[55] E. Sela and J. Malecki, Nonequilibrium conductance of asymmetric nanodevices in the Kondo regime, Phys. Rev. B **80**, 233103 (2009).

[56] A. A. Aligia, Leading temperature dependence of the conductance in Kondo-correlated quantum dots, J. Phys.: Condens. Matter **30**, 155304 (2018).

[57] Y. Nishikawa, O. J. Curtin, A. C. Hewson, D. J. G. Crow, and J. Bauer, Conditions for observing emergent Su(4) symmetry in a double quantum dot, Phys. Rev. B **93**, 235115 (2016).

[58] D. B. Karki, C. Mora, J. von Delft, and M. N. Kiselev, Two-color Fermi-liquid theory for transport through a multilevel Kondo impurity, Phys. Rev. B **97**, 195403 (2018).

[59] Y. Teratani, R. Sakano, and A. Oguri, Fermi liquid theory for nonlinear transport through a multilevel anderson impurity, Phys. Rev. Lett. **125**, 216801 (2020).

[60] Y. Teratani, R. Sakano, T. Hata, T. Arakawa, M. Ferrier, K. Kobayashi, and A. Oguri, Field-induced Su(4) to Su(2) Kondo crossover in a half-filling nanotube dot: Spectral and finite-temperature properties, Phys. Rev. B **102**, 165106 (2020).

[61] A. Georges and Y. Meir, Electronic correlations in transport through coupled quantum dots, Phys. Rev. Lett. **82**, 3508 (1999).

[62] B. Dong and X. L. Lei, Kondo effect and antiferromagnetic correlation in transport through tunneling-coupled double quantum dots, Phys. Rev. B **65**, 241304(R) (2002).

[63] I. J. Hamad, L. Costa Ribeiro, G. B. Martins, and E. V. Anda, Transport properties of a two-impurity system: A theoretical approach, Phys. Rev. B **87**, 115102 (2013).

[64] R. Aguado and D. C. Langreth, Out-of-equilibrium kondo effect in double quantum dots, Phys. Rev. Lett. **85**, 1946 (2000).

[65] R. López, R. Aguado, and G. Platero, Nonequilibrium transport through double quantum dots: Kondo effect versus antiferromagnetic coupling, Phys. Rev. Lett. **89**, 136802 (2002).

[66] N. S. Wingreen and Y. Meir, Anderson model out of equilibrium: Noncrossing-approximation approach to transport through a quantum dot, Phys. Rev. B **49**, 11040 (1994).

[67] M. H. Hettler, J. Kroha, and S. Hershfield, Nonequilibrium dynamics of the Anderson impurity model, Phys. Rev. B **58**, 5649 (1998).

[68] P. Roura Bas and A. A. Aligia, Nonequilibrium transport through a singlet-triplet Anderson impurity, Phys. Rev. B **80**, 035308 (2009).

[69] P. R. Bas and A. A. Aligia, Nonequilibrium dynamics of a singlet-triplet Anderson impurity near the quantum phase transition, J. Phys.: Condens. Matter **22**, 025602 (2009).

[70] S. Florens, A. Freyn, N. Roch, W. Wernsdorfer, F. Balestro, P. Roura-Bas, and A. A. Aligia, Universal transport signatures in two-electron molecular quantum dots: gate-tunable hund's rule, underscreened Kondo effect and quantum phase transitions, J. Phys.: Condens. Matter **23**, 243202 (2011).

[71] G. C. Tettamanzi, J. Verduijn, G. P. Lansbergen, M. Blaauboer, M. J. Calderón, R. Aguado, and S. Rogge, Magnetic-field probing of an Su(4) Kondo resonance in a single-atom transistor, Phys. Rev. Lett. **108**, 046803 (2012).

[72] P. Roura-Bas, L. Tosi, and A. A. Aligia, Replicas of the Kondo peak due to electron-vibration interaction in molecular transport properties, Phys. Rev. B **93**, 115139 (2016).

[73] P. Roura-Bas, F. Güller, L. Tosi, and A. A. Aligia, Destructive quantum interference in transport through molecules with electron-electron and electron-vibration interactions, J. Phys.: Condens. Matter **31**, 465602 (2019).

[74] D.-J. Choi, P. Abufager, L. Limot, and N. Lorente, From tunneling to contact in a magnetic atom: The non-equilibrium Kondo effect, J. Chem. Phys. **146**, 092309 (2016).

[75] P. Roura-Bas, Universal scaling in transport out of equilibrium through a single quantum dot using the noncrossing approximation, Phys. Rev. B **81**, 155327 (2010).

[76] D. M. Fugger, A. Dorda, F. Schwarz, J. von Delft, and E. Arrigoni, Nonequilibrium Kondo effect in a magnetic field: Auxiliary master equation approach, New J. Phys. **20**, 013030 (2018).

[77] D. M. Fugger, D. Bauernfeind, M. E. Sorantin, and E. Arrigoni, Nonequilibrium pseudogap anderson impurity model: A master equation tensor network approach, Phys. Rev. B **101**, 165132 (2020).

[78] A. Rosch, J. Paaske, J. Kroha, and P. Wölfle, Nonequilibrium transport through a Kondo dot in a magnetic field: Perturbation theory and poor man's scaling, Phys. Rev. Lett. **90**, 076804 (2003).

[79] S. G. Jakobs, M. Pletyukhov, and H. Schoeller, Nonequilibrium functional renormalization group with frequency-dependent vertex function: A study of the single-impurity Anderson model, Phys. Rev. B **81**, 195109 (2010).

[80] M. Pletyukhov and H. Schoeller, Nonequilibrium Kondo model: Crossover from weak to strong coupling, Phys. Rev. Lett. **108**, 260601 (2012).

[81] A. Manaparambil, A. Weichselbaum, J. von Delft, and I. Weymann, Nonequilibrium spintronic transport through Kondo impurities, Phys. Rev. B **106**, 125413 (2022).

[82] A. A. Aligia and L. A. Salguero, Magnetotransport through a quantum wire side coupled to a quantum dot, Phys. Rev. B **70**, 075307 (2004).

[83] Th. Pruschke and N. Grewe, The Anderson model with finite coulomb repulsion, Z. Phys. B **74**, 439 (1989).

[84] K. Haule, S. Kirchner, J. Kroha, and P. Wölfle, Anderson impurity model at finite Coulomb interaction U: Generalized noncrossing approximation, Phys. Rev. B **64**, 155111 (2001).

[85] L. Tosi, P. Roura-Bas, A. M. Llois, and L. O. Manuel, Effects of vertex corrections on diagrammatic approximations applied to the study of transport through a quantum dot, Phys. Rev. B **83**, 073301 (2011).

[86] T. A. Costi, J. Kroha, and P. Wölfle, Spectral properties of the Anderson impurity model: Comparison of numerical-renormalization-group and noncrossing-approximation results, Phys. Rev. B **53**, 1850 (1996).

[87] G. S. Kumar, G. Prasad, and R. O. Pohl, Experimental determinations of the Lorenz number, J. Mater. Sci. **28**, 4261 (1993).

[88] P. Roura-Bas, L. Tosi, A. A. Aligia, and K. Hallberg, Interplay between quantum interference and Kondo effects in nonequilibrium transport through nanoscopic systems, Phys. Rev. B **84**, 073406 (2011).

[89] L. Tosi, P. Roura-Bas, and A. A. Aligia, Non-equilibrium conductance through a benzene molecule in the Kondo regime, J. Phys.: Condens. Matter **24**, 365301 (2012).

[90] J. Fernández, F. Lisandrini, P. Roura-Bas, C. Gazza, and A. A. Aligia, Width of the charge-transfer peak in the SU(n) impurity anderson model and its relevance to nonequilibrium transport, Phys. Rev. B **97**, 045144 (2018).

[91] L. Tosi, P. Roura-Bas, and A. A. Aligia, Restoring the su(4) kondo regime in a double quantum dot system, J. Phys.: Condens. Matter **27**, 335601 (2015).

[92] L. Tosi, P. Roura-Bas, and A. A. Aligia, Transition between SU(4) and SU(2) Kondo effect, Phys. B: Condens. Matter **407**, 3259 (2012),.

[93] M. Pustilnik and L. I. Glazman, Kondo effect in real quantum dots, Phys. Rev. Lett. **87**, 216601 (2001).

[94] R. Sánchez and M. Büttiker, Optimal energy quanta to current conversion, Phys. Rev. B **83**, 085428 (2011).

[95] R. Sánchez and M. Büttiker, Detection of single-electron heat transfer statistics, Europhys. Lett. **100**, 47008 (2012).

[96] T. Ruokola and T. Ojanen, Single-electron heat diode: Asymmetric heat transport between electronic reservoirs through Coulomb islands, Phys. Rev. B **83**, 241404(R) (2011).

[97] A. A. Balandina and O. L. Lazarenkova, Mechanism for thermoelectric figure-of-merit enhancement in regimented quantum dot superlattices, Appl. Phys. Lett. **82**, 415 (2003).

[98] R. Allub and A. A. Aligia, Ground state and magnetic susceptibility of intermediate-valence Tm impurities, Phys. Rev. B **52**, 7987 (1995).

[99] N. Roch, S. Florens, V. Bouchiat, W. Wernsdorfer, and F. Balestro, Quantum phase transition in a single-molecule quantum dot, Nature (London) **453**, 633 (2008).

[100] G. Zaránd, C.-H. Chung, P. Simon, and M. Vojta, Quantum criticality in a double-quantum-dot system, Phys. Rev. Lett. **97**, 166802 (2006).

[101] D. P. Daroca, P. Roura-Bas, and A. A. Aligia, Relation between width of zero-bias anomaly and kondo temperature in transport measurements through correlated quantum dots: Effect of asymmetric coupling to the leads, Phys. Rev. B **98**, 245406 (2018).

[102] A. K. Mitchell, M. R. Galpin, and D. E. Logan, Gate voltage effects in capacitively coupled quantum dots, Europhys. Lett. **76**, 95 (2006).

[103] A. F. Otte, M. Ternes, K. von Bergmann, S. Loth, H. Brune, C. P. Lutz, C. F. Hirjibehedin, and A. J. Heinrich, The role of magnetic anisotropy in the Kondo effect, Nat. Phys. **4**, 847 (2008).